

Vortex patterns and the critical rotational frequency in rotating dipolar Bose-Einstein condensates

Yongyong Cai,¹ Yongjun Yuan,^{2,*} Matthias Rosenkranz,³ Han Pu,⁴ and Weizhu Bao³

¹*Beijing Computational Science Research Center, Haidian District, Beijing 100193, People's Republic of China*

²*Key Laboratory of High Performance Computing and Stochastic Information Processing (Ministry of Education of China),
College of Mathematics and Computer Science, Hunan Normal University,
Changsha, Hunan 410081, People's Republic of China*

³*Department of Mathematics, National University of Singapore, 119076, Singapore*

⁴*Department of Physics and Astronomy, and Rice Quantum Institute, Rice University, Houston, TX 77251, USA*

(Dated: January 23, 2018)

Based on the two-dimensional mean-field equations for pancake-shaped dipolar Bose-Einstein condensates in a rotating frame with both attractive and repulsive dipole-dipole interaction (DDI) as well as arbitrary polarization angle, we study the profiles of the single vortex state and show how the critical rotational frequency change with the s-wave contact interaction strengths, DDI strengths and the polarization angles. In addition, we find numerically that at the ‘magic angle’ $\vartheta = \arccos(\sqrt{3}/3)$, the critical rotational frequency is almost independent of the DDI strength. By numerically solving the dipolar GPE at high rotational speed, we identify different patterns of vortex lattices which strongly depend on the polarization direction. As a result, we undergo a study of vortex lattice structures for the whole regime of polarization direction and find evidence that the vortex lattice orientation tends to be aligned with the direction of the dipoles.

PACS numbers: 03.75.Hh, 75.80.+q, 67.85.-d

I. INTRODUCTION

One of the striking features of rotating atomic Bose-Einstein condensates (BECs) is the formation of vortices above a critical angular velocity [1–3]. In a symmetric BEC, multiple vortices arrange in a characteristic triangular pattern [2]. This triangular vortex lattice minimizes the free energy of the BEC.

While the initial experiments considered atoms with local interactions, more recently, dipolar BECs with electric or magnetic dipole moment have received much attention from both theoretical and experimental studies (for recent reviews, see Refs. [4, 5]). Their dipole-dipole interaction (DDI) crucially affects the ground-state properties [6, 7], stability [8–11], and dynamics of the gas [12]. Furthermore, they offer a route for studying many-body quantum effects, such as a superfluid-to-crystal quantum phase transition [13], supersolids [14] or even topological order [15]. Recent advances in experimental techniques have paved the way for a Bose-Einstein condensate (BEC) of ^{52}Cr with a magnetic dipole moment $6\mu_B$ (Bohr magneton μ_B), much larger than conventional alkali BECs [16–18]. Promising candidates for dipolar BEC experiments are Er and Dy with even larger magnetic moments of $7\mu_B$ and $10\mu_B$, respectively, which have been reported in experiments [19, 20]. Furthermore, DDI-induced decoherence and spin textures have been observed in alkali-metal condensates [21, 22]. Dipolar effects also play a crucial role in experiments with Rydberg atoms [23] and heteronuclear molecules [24, 25]. Bosonic heteronuclear molecules may provide a basis for future experiments on BECs with dipole moments much larger than in atomic BECs [26].

The anisotropy of the dipole-dipole interactions crucially affects stationary states of the rotating dipolar BEC. In this ar-

ticle we focus on a system of dipolar BEC confined in a quasi-two-dimensional pancake shaped trapping potential with the atomic magnetic dipoles polarized by an external magnetic field. We define the polarization angle ϑ to be the angle between the dipoles and the direction normal to the plane of the condensate. Hence, if the dipoles lie in the plane of the condensate, we have $\vartheta = \pi/2$; whereas if the dipoles are perpendicular to the plane, we have $\vartheta = 0$. By adjusting the external magnetic field, ϑ can be varied smoothly between 0 and $\pi/2$. Most previous studies of rotating dipolar BECs focused only on the two limiting cases with $\vartheta = 0$ or $\pi/2$ [27–31]. Recently, Zhao and Gu [32] and Malet *et al.* [33] studied the angular momentum and critical rotational frequency of a 2D dipolar BEC with positive DDI strength in this intermediate regime. Their results show that the critical rotational frequency increases with the polarization angle ϑ , while the relation between the critical rotational velocity and the DDI strength is dependent of the polarization angles. Martin *et al.* [34] analytically studied the vortex lattice for the case where the dipoles are not perpendicular to the plane of rotation, and suggested there is a phase transition in the vortex geometry from triangular to square which can be measured as a function of the DDI strength, whereas the vortex orientation is independent of the polarization angle ϑ . This vortex structure transition was observed in the numerical results of Zhao and Gu [32] for a rotating quasi-2D dipolar BEC with positive DDI strength, however, to our knowledge, there have not, to date, been numerical results concerning the change of vortex lattice orientation with the polarization angle ϑ . In this paper, we further study the effect of the s-wave contact interaction strength and the polarization angle on the critical rotational frequency with both attractive and repulsive DDI, and focus on fast rotation with many vortices. We observe different patterns of vortex lattices which strongly depend on the polarization direction and illustrate the vortex orientation by virtue of the static structure factor [35, 36]. We also take into

* Corresponding Author

account attractive DDI which can be achieved with a rotating magnetic field [37]. Simulating high vortex numbers requires reliable numerical methods. Spectral methods are very accurate for such kinds of problems [38–42], with less grid points needed than those of traditional finite difference methods.

This article is organized as follows. In Sec. II we present a 2D model for a dipolar BEC in the rotating frame. We also explain our approach for solving this model numerically. In Sec. III, we show how the s-wave contact interaction strength and the polarization angle affect the critical rotational frequency with both attractive and repulsive DDI strengths. In Sec. IV we present simulation results of stationary states at high rotation frequency for different polarization angles and DDI strengths. Focusing on the regime with many vortices allows us to discern characteristic vortex patterns that occur as the polarization changes from predominantly perpendicular to parallel. We conclude in Sec. V.

II. MODEL

We consider a polarized dipolar BEC trapped in a harmonic potential $V(\mathbf{r}) = \frac{1}{2}m[\omega_r^2(x^2 + y^2) + \omega_z^2 z^2]$ with m the atomic mass and ω_r, ω_z the transverse and axial trap frequencies, respectively. We assume that the magnetic dipoles are polarized along an axis $\mathbf{n} = (\cos \varphi \sin \vartheta, \sin \varphi \sin \vartheta, \cos \vartheta)$, where φ and ϑ are the azimuthal and polar angles, respectively. The DDI potential between two atoms separated by the relative vector \mathbf{r} is given by

$$U_{\text{dd}}(\mathbf{r}) = \frac{g_d}{4\pi} \frac{1 - 3 \cos^2 \theta}{|\mathbf{r}|^3}. \quad (1)$$

Here, θ is the angle between the polarization axis and \mathbf{r} . For magnetic dipoles the interaction strength g_d is given by $g_d = \mu_0 \mu_d^2$, where μ_0 is the magnetic vacuum permeability and μ_d the dipole moment. In addition, we assume that

the BEC is rotating with frequency Ω around the z axis. In the remainder of this article we adopt length, time and energy units as $a_r = \sqrt{\hbar/m\omega_r}$, $1/\omega_r$, and $\hbar\omega_r$, respectively. At zero temperature this system is described by the Gross-Pitaevskii equation (GPE) in the rotating frame [12, 43]

$$i\partial_t \Psi(\mathbf{r}, t) = \left[-\frac{1}{2} \nabla^2 + V(\mathbf{r}) - \Omega L_z + g |\Psi|^2 + \int d\mathbf{r}' U_{\text{dd}}(\mathbf{r} - \mathbf{r}') |\Psi(\mathbf{r}', t)|^2 \right] \Psi(\mathbf{r}, t). \quad (2)$$

Here, $L_z = i(y\partial_x - x\partial_y)$ is the z component of the angular momentum operator and $g = 4\pi N a_s / a_r$ with N being the number of atoms and a_s being the s-wave scattering length. The dimensionless DDI strength is given by $g_d = Nm\mu_0\mu_d^2/3\hbar^2 a_r$.

We only consider the case where $\omega_z \gg \omega_r$ and the contact and dipole-dipole interaction energies are smaller than $\hbar\omega_z$ such that the BEC remains in the ground state of the axial harmonic trap. This is the limit of a quasi-2D BEC [44]. The wave function $\Psi(\mathbf{r}, t)$ can be separated into a radial and longitudinal part, that is, $\Psi(\mathbf{r}, t) = \psi(\boldsymbol{\rho}, t)w(z) \exp(-i\gamma t/2)$ with $\boldsymbol{\rho} = (x, y)$, $|\boldsymbol{\rho}| = \sqrt{x^2 + y^2}$, $w(z) = (\gamma/\pi)^{1/4} \exp(-z^2/2\gamma)$, and $\gamma = \omega_z/\omega_r$. Inserting this expansion of the wave function into Eq. (2) and integrating out the z axis reduces Eq. (2) to [45, 46]

$$i\partial_t \psi(\boldsymbol{\rho}, t) = \left[-\frac{1}{2} \nabla_r^2 + \frac{|\boldsymbol{\rho}|^2}{2} - \Omega L_z + \bar{g} |\psi(\boldsymbol{\rho}, t)|^2 + \int d\boldsymbol{\rho}' U_{\text{dd}}^{2\text{D}}(\boldsymbol{\rho} - \boldsymbol{\rho}') |\psi(\boldsymbol{\rho}', t)|^2 \right] \psi(\boldsymbol{\rho}, t). \quad (3)$$

Here, $\nabla_r^2 = \partial_x^2 + \partial_y^2$ and $\bar{g} = \sqrt{\frac{\gamma}{2\pi}} [g - g_d(1 - 3 \cos^2 \vartheta)]$ is the effective 2D contact interaction that now depends on the DDI strength and polarization direction. The effective kernel for the 2D DDI is given by

$$U_{\text{dd}}^{2\text{D}}(\boldsymbol{\rho}) = \frac{g_d \gamma^{3/2}}{8\sqrt{2\pi^3}} e^{\gamma|\boldsymbol{\rho}|^2/4} \left[(1 - 3 \cos^2 \vartheta + \gamma[(x \cos \varphi + y \sin \varphi)^2 \sin^2 \vartheta - |\boldsymbol{\rho}|^2 \cos^2 \vartheta]) K_0(\gamma|\boldsymbol{\rho}|^2/4) - (1 - \cos^2 \vartheta + \gamma[(x \cos \varphi + y \sin \varphi)^2 [1 - 2/\gamma|\boldsymbol{\rho}|^2] \sin^2 \vartheta - |\boldsymbol{\rho}|^2 \cos^2 \vartheta]) K_1(\gamma|\boldsymbol{\rho}|^2/4) \right], \quad (4)$$

where K_ν are modified Bessel functions of the second kind. In Fourier space the DDI [potential in second line in Eq. (3)] becomes $\hat{V}_{2\text{D}}(\mathbf{k}) = \hat{U}_{2\text{D}}(\mathbf{k}) |\hat{\psi}(\mathbf{k})|^2$ with $\hat{\psi}(\mathbf{k})$ being the condensate wave function in momentum space and $\hat{U}_{2\text{D}}(\mathbf{k}) = \frac{3g_d}{2} [(\hat{k}_x \cos \varphi + \hat{k}_y \sin \varphi)^2 \sin^2 \vartheta - \cos^2 \vartheta] k e^{k^2/2\gamma} \text{erfc}(k/\sqrt{2\gamma})$, where $k = |\mathbf{k}|$, $\hat{k}_{x,y} = k_{x,y}/k$ are normalized components of the momentum, and $\text{erfc}(x) = 1 - \text{erf}(x)$ is the complementary error function.

The effective nonlocal interaction of a quasi-2D dipolar BEC, Eq. (4), is attractive along the projection of the polarization axis $(\cos \varphi, \sin \varphi)$ and repulsive perpendicular to the

polarization axis. For axial polarization $\vartheta = 0$, the nonlocal interaction is isotropic and repulsive. In our work, without loss of generality, we assume that the dipoles are polarized in the xz -plane, such that we can fix $\varphi = 0$. The effective interaction diverges less strongly in the limit $|\boldsymbol{\rho}| \rightarrow 0$ than the full 3D dipole-dipole potential U_{dd} . Furthermore, it has a well-behaved Fourier transform, which is advantageous for numerical computations [45]. To find the ground states, we use the imaginary time method, with backward Euler discretization in time and Fourier spectral discretization in space. In our calculation, the effective 2D nonlocal term is evaluated by Fast Fourier Transform. When the total energy attains its

global minimum by the imaginary time proration [38–40], the ground state is obtained.

III. CRITICAL ROTATIONAL FREQUENCY

In this section, we show the impact of varying s-wave contact interaction strength g , DDI strength g_d and polarization angle ϑ to the critical rotational frequency, respectively. Actually, Malet *et al.* [33] have studied the angular momentum and critical rotational frequency of a dipolar BEC in the intermediate regime with positive DDI strength, here we further study it for rotating dipolar BECs with both positive and negative DDI. We are also interested in the change of single vortex shape with different polarization angle ϑ .

Figures 1–2 show density contour plots of the rotating dipolar BEC for different polarization angles ϑ and rotational frequency Ω with negative and positive DDI strength g_d , respectively. It is observed that for the fixed effective 2D contact interaction strength \bar{g} and the kernel $U_{dd}^{2D}(\rho)$ for the DDI in Eq. (3), there exists a critical rotational frequency Ω_c such that there is no vortex if $\Omega < \Omega_c$ and at least one vortex if $\Omega \geq \Omega_c$ [cf. e.g., Figs. 1(a)–(b) and 2(e)–(f)]. Thus vortex patterns are formed after the rotational frequency exceeding its critical value. Furthermore, the shape of the vortices change with the polarization angle ϑ . It is found that the vortex core is no longer radially symmetric and turns more and more flat along the y -axis (the x -axis) for negative (positive) DDI strength g_d . From the Fourier transform of U_{dd}^{2D} (4), we can show that the DDI interaction potential becomes more and more repulsive (attractive) in the x direction when ϑ increases from 0 to $\frac{\pi}{2}$ for positive (negative) g_d . As a consequence of such anisotropic property of DDI in 2D, the density of the ground state are more concentrated in the y direction for positive g_d and in the x direction for negative g_d . In contrast, when $g_d = 0$ or $\vartheta = 0$, the DDI in the 2D rotating dipolar BEC Eq. (3) is isotropic in the xy -plane, and the vortices in both cases possess radial symmetry in shape.

Figure 3 illustrates the change of critical rotational frequency Ω_c with varying s-wave contact interaction strength g , when the polarization direction is perpendicular to the rotating plane. The numerical results show that Ω_c decreases when g increases for any fixed positive and negative DDI strength g_d . Further, $\Omega_c \rightarrow 1$ as $g \rightarrow 0$ and Ω_c drops dramatically when g increases near the boundary $g \approx 0$. This is in accordance with the conventional rotating condensates without DDI [1–3]. It is also clear that when the DDI strength $g_d \nearrow$, $\Omega_c \searrow$ for any fixed s-wave contact interaction strength g and other parameters.

Figure 4 shows the critical rotational frequency Ω_c versus the polarization angle ϑ . The numerical results show that Ω_c decreases (increases) when ϑ varies from 0 to $\pi/2$ for any fixed negative (positive) DDI strength g_d . Moreover, the curves of Ω_c as functions of ϑ with both negative and positive DDI strength g_d almost intersect with each other at the ‘magic angle’ $\vartheta = \arccos(\sqrt{3}/3)$, since at this angle the effective 2D contact interaction in Eq. (3) is independent of the DDI strength g_d and the DDI is much smaller compared to the

effective 2D contact interaction thus has very little effect on the critical rotational frequency.

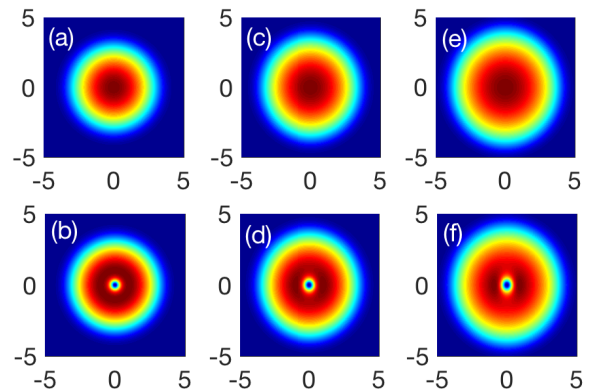


FIG. 1. (Color online) Density of a rotating dipolar BEC for fixed $\gamma = 10$, $g = 250$, $g_d = -100$, different polarization angles and rotation frequency. (a) $\varphi = \vartheta = 0$ and $\Omega = 0.356$. (b) $\varphi = \vartheta = 0$ and $\Omega = 0.357$. (c) $\varphi = 0$, $\vartheta = \pi/4$ and $\Omega = 0.275$. (d) $\varphi = 0$, $\vartheta = \pi/4$ and $\Omega = 0.276$. (e) $\varphi = 0$, $\vartheta = \pi/2$ and $\Omega = 0.236$. (f) $\varphi = 0$, $\vartheta = \pi/2$ and $\Omega = 0.237$.

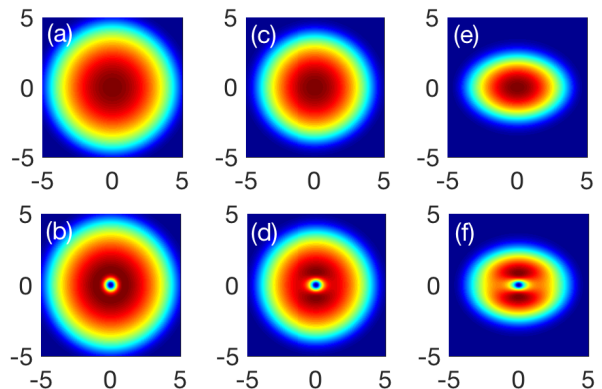


FIG. 2. (Color online) Density of a rotating dipolar BEC for fixed $\gamma = 10$, $g = 250$, $g_d = 200$, different polarization angles and rotation frequency. (a) $\varphi = \vartheta = 0$ and $\Omega = 0.195$. (b) $\varphi = \vartheta = 0$ and $\Omega = 0.196$. (c) $\varphi = 0$, $\vartheta = \pi/4$ and $\Omega = 0.232$. (d) $\varphi = 0$, $\vartheta = \pi/4$ and $\Omega = 0.233$. (e) $\varphi = 0$, $\vartheta = \pi/2$ and $\Omega = 0.357$. (f) $\varphi = 0$, $\vartheta = \pi/2$ and $\Omega = 0.358$.

IV. VORTEX PATTERNS

In this section, we show different vortex lattices that emerge as stationary states for varying polarization angles under fast rotation. To characterize the structure of the vortex lattice, we define the static structure factor [35, 36]

$$S(\mathbf{k}) = \frac{1}{N_v^2} \left| \sum_j e^{i\mathbf{k} \cdot \rho_j} \right|^2, \quad (5)$$

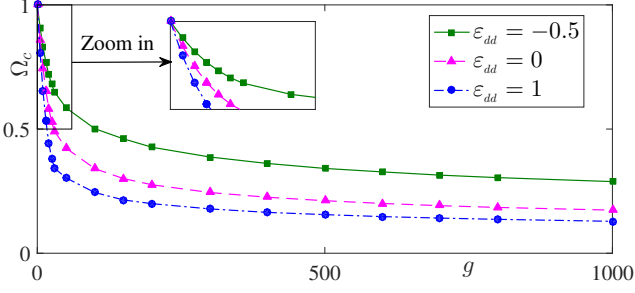


FIG. 3. The change of critical rotation frequency Ω_c of a rotating dipolar BEC with the s-wave contact interaction strength g for fixed $\gamma = 10$, $\mathbf{n} = (\mathbf{0}, \mathbf{0}, 1)$ and a natural dimensionless parameter $\varepsilon_{dd} := g_d/g = -0.5, 0$ and 1 , respectively.

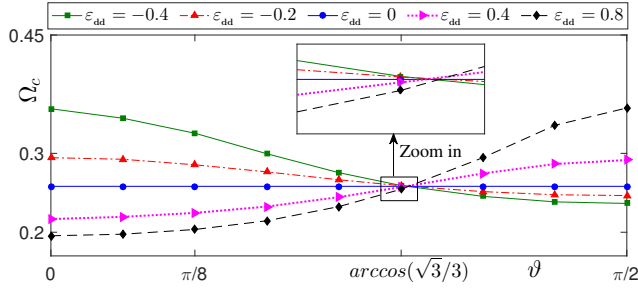


FIG. 4. The change of critical rotation frequency Ω_c of a rotating dipolar BEC with the polarization angle ϑ for fixed $\gamma = 10$, $g = 250$ and $\varepsilon_{dd} = -0.4, -0.2, 0, 0.4$ and 0.8 , respectively.

where N_v is the number of vortices and ρ_j are their positions. The structure factor exhibits peaks at the reciprocal lattice sites, which reveal the frequencies and orientation of the vortex lattice. The reciprocal lattice is defined by two basis vectors \mathbf{k}_1 and \mathbf{k}_2 . Here we choose \mathbf{k}_1 as the one closest to the y -axis and use the parameter $\eta = \angle(\mathbf{k}_1, \mathbf{k}_2)$ to characterize the orientation of the vortex lattice [c.f. Fig. 5]. $\eta = \pi/2$ for a rectangular vortex lattice, and $\pi/3$ for a triangular lattice.

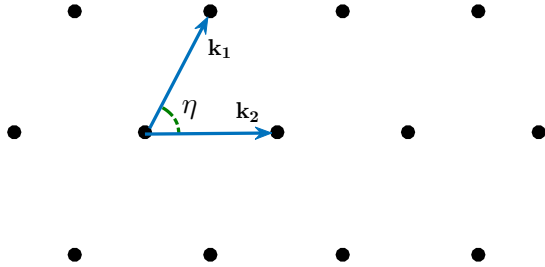


FIG. 5. Illustration of the Bravais lattice basis vectors and the lattice parameters.

We start with the impact of the polarization direction on the

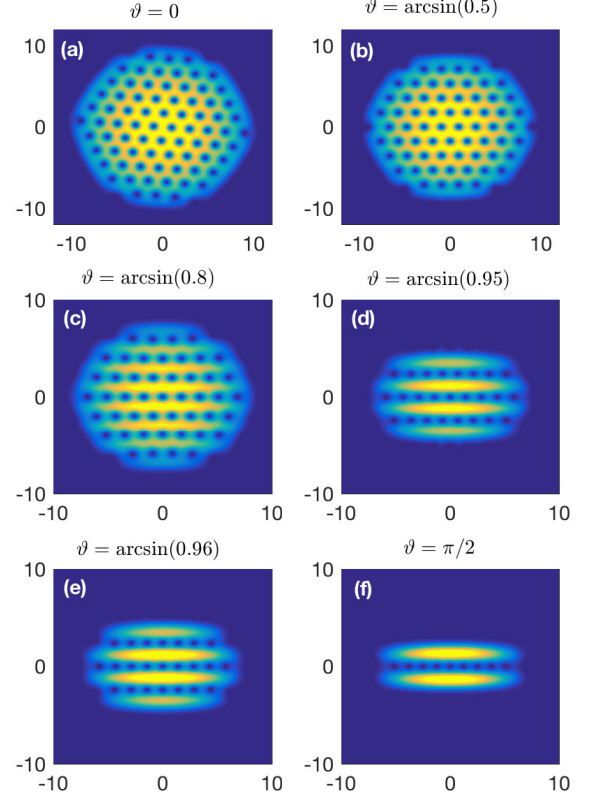


FIG. 6. (Color online) Density of a rotating dipolar BEC for different polarization angles. $\varphi = 0$ and $\vartheta = 0, \arcsin(0.5), \arcsin(0.8), \arcsin(0.95), \arcsin(0.96), \pi/2$ (from left to right, top to bottom). The rotation frequency is $\Omega/\omega_r = 0.95$, $\gamma = 10$, $g = 250$, and $g_d = 250$.

vortex lattice geometry under the fast rotation. We compute the ground states of the dipolar BEC for different polarization angles ϑ at strong DDI $g_d = g$ and high rotation frequency $\Omega/\omega_r = 0.95$ by imaginary time propagation. As shown in Fig. 6, for polarization predominantly along the symmetry axis of the BEC (i.e., $\vartheta \approx 0$), the vortices form a regular triangular lattice [cf. Figs. 6(a)–(d)]. The corresponding structure factor in Figs. 8(a)–(d) reveals a hexagonal reciprocal primitive cell, characteristic of the triangular lattice. As the polarization axis rotates into the plane of the BEC, the vortex lattice aligns with the polarization [cf. Figs. 6(c)–(f)]. Parallel polarization (i.e., $\vartheta \approx \pi/2$) is shown in Figs. 6(e)–(f). In the extreme case $\vartheta = \pi/2$, the vortices align on a central 1D lattice that splits the BEC. The elongation in each BEC fragment is caused by magnetostriction, which tends to align dipoles in a head-to-tail configuration. The DDI between the two fragments is repulsive but drops exponentially [47, 48]. The distance between the fragments is $\simeq 2.5a_r$, which is on the order of μm . The corresponding static structure factor in Fig. 8(f) is nearly uniform in the perpendicular direction and periodic along the polarization direction. For polarization

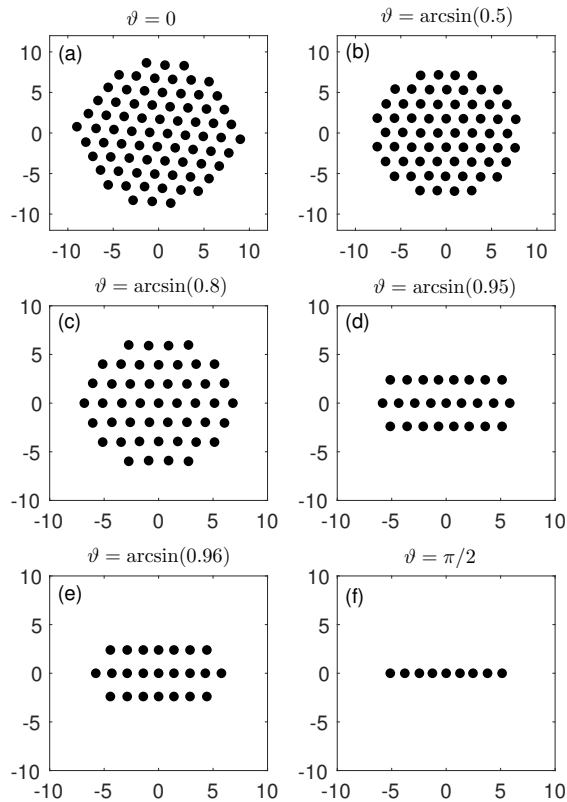


FIG. 7. Vortex positions. Same parameters as in Fig. 6.

angles which are slightly less than $\pi/2$, instead of a single split we observe splits into several BEC fragments caused by a nearly rectangular vortex lattice [cf. Figs. 6(e)]. In this configuration the BEC minimizes its energy by forming quasi-1D tubes between the vortices aligned along the polarization direction. Again, the orientation of these tubes is dictated by magnetostriction.

Positions of vortex cores are displayed in Fig. 7. If the polarization is predominantly perpendicular to the rotating plane, the vortex lattice is regular, as observed in the rotating BEC without DDI [1–3, 49–51]. For increasing polarization in the plane, it changes orientation to align with the polarization direction. Rotating the polarization further into the plane, magnetostriction elongates the BEC. Consequently, the vortex lattice becomes more irregular as rows of vortices perpendicular to the polarization are shaved off.

The effective contact interaction \bar{g} in 2D dipolar GPE (3) changes while ϑ varies from 0 to $\pi/2$. When $\varepsilon_{dd} > 0$, \bar{g} is decreasing; when $\varepsilon_{dd} < 0$, \bar{g} is increasing. Based on the conventional rotating BEC results, the number of vortices increases when \bar{g} becomes larger, and Fig. 6 suggests it is also the case for BEC with DDI. In Fig. 9, we show density contour plots of the rotating dipolar BEC for different polarization angles ϑ and different DDI strength with a very fast rotation frequency $\Omega/\omega_r = 0.99$, which nearly equals to its ultimate

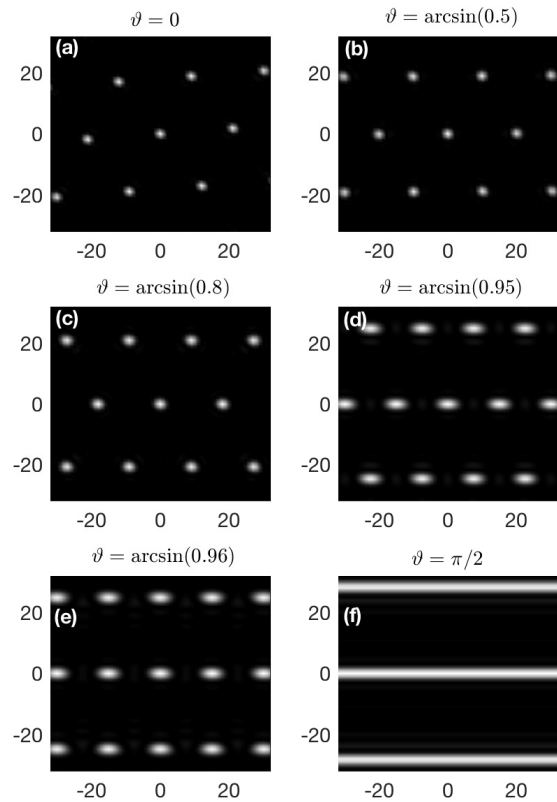


FIG. 8. Static structure factor S . Same parameters as in Fig. 6.

limit $\Omega/\omega_r = 1.0$. It is observed that the change of a triangular vortex lattice structure to a rectangular vortex lattice structure occurs when both the polarization angle ϑ and the natural dimensionless parameter $\varepsilon_{dd} := g_d/g$ are close to their limits $\vartheta = \pi/2$ and $\varepsilon_{dd} = 1.0$. We also found that for dipoles oriented along the z -axis, the system has rotational symmetry. Therefore, the patterns plotted in Fig. 9 with $\vartheta = 0$ can be rotated about the z -axis by an arbitrary angle, while for the other dipole orientations in the xz -plane, the system has a symmetry axis along the y -axis, thus the vortex lattices shown in Fig. 9 with $\vartheta \in (0, \pi/2]$ all obey this symmetry. For the negative DDI strength, there are more vortices found in the condensate for in-plane polarization of the DDI rather than off-plane polarizations, which is in contrast with the positive DDI strength case but agrees well with the behaviour of effective contact interaction \bar{g} . Figs. 6 and 9 imply that the number of vortices are still mainly determined by the effective contact interaction \bar{g} . On the other hand, the DDI in-plane significantly affects the distribution of the vortices (cf. Figs. 8 and 9). When switching to a negative DDI in Fig. 9, we find that in the extreme case $\vartheta = \pi/2$, the shapes of the vortex lattices are much different, i.e., the major axis of the lattice with negative DDI strengths is perpendicular to the polarization x axis, while the major axis of the lattice with positive DDI strengths is parallel to the polarization x axis.

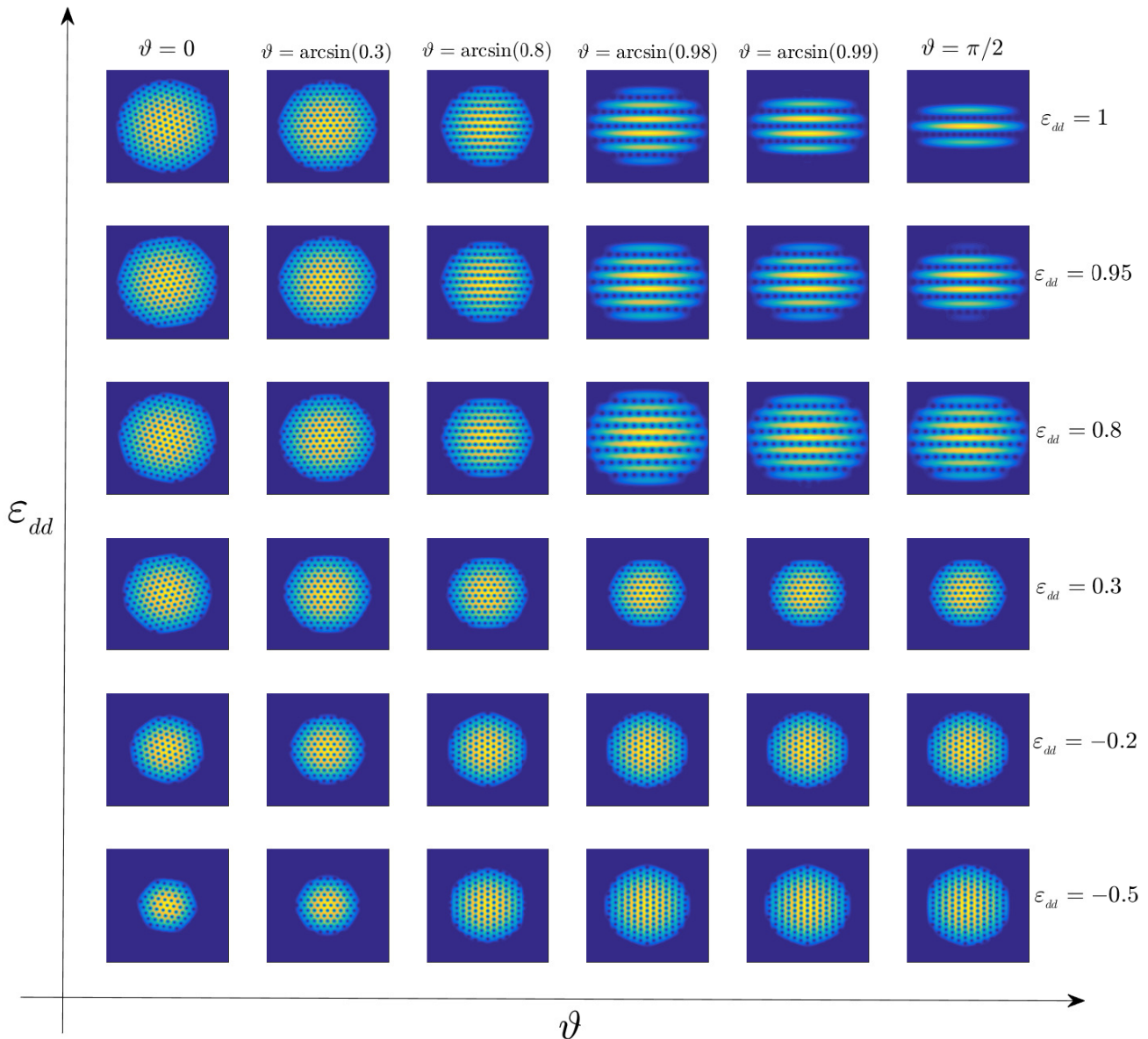


FIG. 9. (Color online) Density of a rotating dipolar BEC for different polarization angles with $\varphi = 0$ and $\vartheta = 0, \arcsin(0.3), \arcsin(0.8), \arcsin(0.98), \arcsin(0.99), \pi/2$ (from left to right) and for different DDI strengths with $\varepsilon_{dd} = -0.5, -0.2, 0.3, 0.8, 0.95, 1.0$ (from bottom to top). The rotation frequency is $\Omega/\omega_r = 0.99$, $\gamma = 10$ and $g = 250$.

We use the parameter η as a function of the polarization angle ϑ , as shown in Fig. 10, to characterize the structural change of the pattern of the vortex lattice for both positive and negative DDI interaction strength. For positive DDI strength, as ϑ increases from 0, η starts from $\pi/3$ and varies rather slowly initially. However, at a critical angle around $\arcsin(0.95)$, η exhibits a jump to the value of $\pi/2$, indicating a structural change to a rectangular vortex lattice. By contrast, for negative DDI strength, η stays near $\pi/3$ as ϑ changes from 0 to $\pi/2$, hence the vortex lattice remains roughly triangular independent of the polarization angle in this case.

V. CONCLUSIONS

We have studied the change of critical rotation frequency versus the s-wave contact interaction strengths, DDI strengths and the varying polarization angles. We find that the critical rotation frequency is monotonously decreasing with growing s-wave contact interaction strength g , and identically approaches the confinement frequency limit for $g \approx 0$ and arbitrary DDI strength g_d . The critical rotation frequency changes very rapidly near $g = 0$ and then decreases more and more slowly for large g . In contrast to previous works, our results

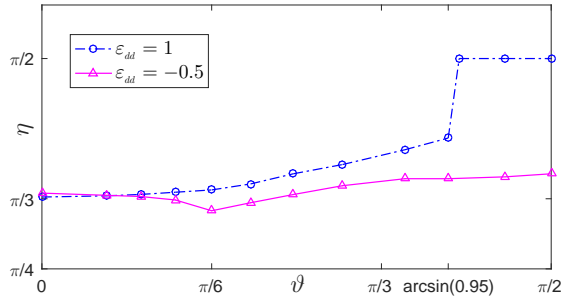


FIG. 10. Lattice orientation parameter η vs ϑ . Same parameters as in Fig. 6.

cover both the case of $g_d > 0$ and $g_d < 0$, thus it is observed that the effect of the polarization angle ϑ to the critical rotation frequency is dependent of the sign of g_d , i.e., the critical rotation frequency increases (decreases) with ϑ from 0 to $\pi/2$ for fixed positive (negative) g_d . In addition, we find numerically that at the ‘magic angle’ $\vartheta = \arccos(\sqrt{3}/3) \approx 54.7^\circ$, the critical rotational frequency is almost independent of the value of DDI strength.

We have numerically simulated the dipolar GPE with fast rotation and show different patterns of vortex lattices which strongly depend on the polarization direction. When the polarization angle ϑ changes from perpendicular to parallel to the condensate plane, a structural phase transition in the vortex geometry from triangular to square is observed for positive g_d , but not for negative g_d . This result is consistent with the analytical results of Martin *et al.* [34]. Meanwhile, by plotting the static structure factor and the orientation parameter η of the vortex lattice, we find evidence that the lattice orientation varies with the polarization angle ϑ . Particularly when $\vartheta = \pi/2$, a vortex lattice which is nearly uniform in the perpendicular direction and periodic along the polarization direction is obtained.

ACKNOWLEDGMENTS

This work was partially supported by the National Natural Science Foundation of China Grants 11771036 and U1530401 (Y.C.), 11601148 (Y.Y.), the Academic Research Fund of Ministry of Education of Singapore grant R-146-000-223-112 (M.R. and W.B.) and the US NSF and the Welch Foundation Grant No. C-1669 (H.P.).

-
- [1] A. J. Leggett, *Rev. Mod. Phys.* **73**, 307 (2001).
 - [2] A. L. Fetter, *Rev. Mod. Phys.* **81**, 647 (2009).
 - [3] H. Saarikoski, S. M. Reimann, A. Harju, and M. Manninen, *Rev. Mod. Phys.* **82**, 2785 (2010).
 - [4] T. Lahaye, C. Menotti, L. Santos, M. Lewenstein, and T. Pfau, *Rep. Prog. Phys.* **72**, 126401 (2009).
 - [5] M. A. Baranov, *Phys. Rep.* **464**, 71 (2008).
 - [6] K. Góral, K. Rzążewski, and T. Pfau, *Phys. Rev. A* **61**, 051601 (2000).
 - [7] S. Yi and L. You, *Phys. Rev. A* **61**, 041604 (2000).
 - [8] L. Santos, G. V. Shlyapnikov, P. Zoller, and M. Lewenstein, *Phys. Rev. Lett.* **85**, 1791 (2000).
 - [9] L. Santos, G. V. Shlyapnikov, and M. Lewenstein, *Phys. Rev. Lett.* **90**, 250403 (2003).
 - [10] U. R. Fischer, *Phys. Rev. A* **73**, 031602 (2006).
 - [11] R. M. W. van Bijnen, D. H. J. O’Dell, N. G. Parker, and A. M. Martin, *Phys. Rev. Lett.* **98**, 150401 (2007).
 - [12] S. Yi and L. You, *Phys. Rev. A* **63**, 053607 (2001).
 - [13] H. P. Büchler, E. Demler, M. Lukin, A. Micheli, N. Prokof’ev, G. Pupillo, and P. Zoller, *Phys. Rev. Lett.* **98**, 060404 (2007).
 - [14] K. Góral, L. Santos, and M. Lewenstein, *Phys. Rev. Lett.* **88**, 170406 (2002).
 - [15] A. Micheli, G. K. Brennen, and P. Zoller, *Nat. Phys.* **2**, 341 (2006).
 - [16] A. Griesmaier, J. Werner, S. Hensler, J. Stuhler, and T. Pfau, *Phys. Rev. Lett.* **94**, 160401 (2005).
 - [17] J. Stuhler, A. Griesmaier, T. Koch, M. Fattori, T. Pfau, S. Giovanazzi, P. Pedri, and L. Santos, *Phys. Rev. Lett.* **95**, 150406 (2005).
 - [18] T. Koch, T. Lahaye, J. Metz, B. Fröhlich, A. Griesmaier, and T. Pfau, *Nat. Phys.* **4**, 218 (2008).
 - [19] K. Aikawa, A. Frisch, M. Mark, S. Baier, A. Rietzler, R. Grimm, and F. Ferlaino, *Phys. Rev. Lett.* **108**, 210401 (2012).
 - [20] M. Lu, N. Q. Burdick, S. H. Youn, and B. L. Lev, *Phys. Rev. Lett.* **107**, 190401 (2011).
 - [21] M. Fattori, G. Roati, B. Deissler, C. D’Errico, M. Zaccanti, M. Jona-Lasinio, L. Santos, M. Inguscio, and G. Modugno, *Phys. Rev. Lett.* **101**, 190405 (2008).
 - [22] M. Vengalattore, S. R. Leslie, J. Guzman, and D. M. Stamper-Kurn, *Phys. Rev. Lett.* **100**, 170403 (2008).
 - [23] T. Vogt, M. Viteau, J. Zhao, A. Chotia, D. Comparat, and P. Pillet, *Phys. Rev. Lett.* **97**, 083003 (2006).
 - [24] K. Ni, S. Ospelkaus, D. Wang, G. Quemener, B. Neyenhuis, M. H. G. de Miranda, J. L. Bohn, J. Ye, and D. S. Jin, *Nature* **464**, 1324 (2010).
 - [25] M. H. G. de Miranda, A. Chotia, B. Neyenhuis, D. Wang, G. Quemener, S. Ospelkaus, J. L. Bohn, J. Ye, and D. S. Jin, *Nat. Phys.* **7**, 502 (2011).
 - [26] A. Voigt, M. Taglieber, L. Costa, T. Aoki, W. Wieser, T. W. Hänsch, and K. Dieckmann, *Phys. Rev. Lett.* **102**, 020405 (2009).
 - [27] N. R. Cooper, E. H. Rezayi, and S. H. Simon, *Phys. Rev. Lett.* **95**, 200402 (2005).
 - [28] N. R. Cooper, E. H. Rezayi, and S. H. Simon, *Solid State Commun.* **140**, 046 (2006).
 - [29] J. Zhang and H. Zhai, *Phys. Rev. Lett.* **95**, 200403 (2005).
 - [30] S. Yi and H. Pu, *Phys. Rev. A* **73**, 061602 (2006).
 - [31] Y. Zhao, J. An, and C.-D. Gong, *Phys. Rev. A* **87**, 013605 (2013).
 - [32] Q. Zhao and Q. Gu, *Chin. Phys. B* **1**, 016702 (2016).
 - [33] F. Malet, T. Kristensen, S. M. Reimann, and G. M. Kavoulakis, *Phys. Rev. A* **83**, 033628 (2011).
 - [34] A. M. Martin, N. G. Marchant, D. H. J. O’Dell, and N. G. Parker, *J. Phys.: Condens. Matter* **29**, 103004 (2017).
 - [35] C. Reichhardt, C. J. Olson, R. T. Scalettar, and G. T. Zimny,

- [Phys. Rev. B **64**, 144509 \(2001\)](#).
- [36] H. Pu, L. O. Baksmaty, S. Yi, and N. P. Bigelow, [Phys. Rev. Lett. **94**, 190401 \(2005\)](#).
- [37] S. Giovanazzi, A. Görlitz, and T. Pfau, [Phys. Rev. Lett. **89**, 130401 \(2002\)](#).
- [38] W. Bao and Y. Cai, [Kinet. Relat. Models **6**, 135 \(2013\)](#).
- [39] W. Bao, Y. Cai, and H. Wang, [J. Comput. Phys. **229**, 7874 \(2010\)](#).
- [40] W. Bao, Q. Tang, and Y. Zhang, [Commun. Comput. Phys. **19**, 37s \(2016\)](#).
- [41] Z. Huang, P. A. Markowich, and C. Sparber, [Kinet. Relat. Mod. **3**, 181 \(2010\)](#).
- [42] X. Antoine, Q. Tang, and Y. Zhang, [Commun. Comput. Phys. \(2017\), to appear](#).
- [43] L. Pitaevskii and S. Stringari, *Bose-Einstein Condensation* (Oxford University Press, Oxford, 2003).
- [44] D. S. Petrov, M. Holzmann, and G. V. Shlyapnikov, [Phys. Rev. Lett. **84**, 2551 \(2000\)](#).
- [45] Y. Cai, M. Rosenkranz, Z. Lei, and W. Bao, [Phys. Rev. A **82**, 043623 \(2010\)](#).
- [46] S. Yi and H. Pu, [Phys. Rev. A **73**, 061602 \(2006\)](#).
- [47] M. A. Baranov, A. Micheli, S. Ronen, and P. Zoller, [Phys. Rev. A **83**, 043602 \(2011\)](#).
- [48] M. Rosenkranz and W. Bao, [Phys. Rev. A **84**, 050701 \(2011\)](#).
- [49] A. Aftalion and Q. Du, [Phys. Rev. A **64**, 063603 \(2001\)](#).
- [50] W. Bao, H. Wang, and P. A. Markowich, [Commun. Math. Sci. **3**, 57 \(2005\)](#).
- [51] R. Zeng and Y. Zhang, [Computer Physics Communications **180**, 854 \(2009\)](#).